A Pressure Projection Method for Nearly Incompressible Rubber Hyperelasticity, Part II: Applications

Jiun-Shyan Chen
Assistant Professor,
Mem. ASME.

Cheng-Tang Wu
Research Assistant.

Chunhui Pan
Research Assistant.

Department of Mechanical Engineering
and Center for Computer-Aided Design,
The University of Iowa,
2133 Engineering Building,
Iowa City, IA 52242-1527

In the first part of this paper a pressure projection method was presented for the nonlinear analysis of structures made of nearly incompressible hyperelastic materials. The main focus of the second part of the paper is to demonstrate the performance of the present method and to address some of the issues related to the analysis of engineering elastomers including the proper selection of strain energy density functions. The numerical procedures and the implementation to nonlinear finite element programs are presented. Mooney-Rivlin, Cubic, and Modified Cubic strain energy density functions are used in the numerical examples. Several classical finite elasticity problems as well as some practical engineering elastomer problems are analyzed. The need to account for the slight compressibility of rubber (finite bulk modulus) in the finite element formulation is demonstrated in the study of apparent Young's modulus of bonded thin rubber units. The combined shear-bending deformation that commonly exists in rubber mounting systems is also analyzed and discussed.

1 Introduction

In most engineering elastomeric applications, rubber components experience strains in the order of several hundred percent. The amount of computation involved in the finite element analysis is tremendous and therefore an accurate and efficient finite element formulation is highly desirable. In Part I of this paper, a least-squares-based pressure projection method was introduced. The formulation was developed in a general framework such that it provides flexibility for the degeneration to other existing formulations. As a result, the expression of the resulting tangent stiffness matrix is rather complex. In this paper, condensed numerical procedures for code implementation are presented so that some of the separately integrated tangent stiffness matrices and force vectors are formed at once to provide better computational efficiency.

In addition to a reliable finite element formulation, an appropriate strain energy density function capable of describing rubber behavior under large strain is essential to the success of nonlinear finite element analysis. Although Mooney-Rivlin strain energy function has been widely used in many finite element formulations such as those in Scharnhorst and Pian (1978), Liu et al. (1988) and Chang et al. (1991), the study by Tschoegl (1971) and James et al. (1975a, b) suggested that the popular Mooney-Rivlin model is not adequate to describe rubber behavior under very large and complex deformations. Yeoh (1993) proposed a Cubic strain energy density function as a correction of the Mooney-Rivlin function to capture the nonlinear shear behavior of rubber at large strain. This function was later modified by adding an additional exponential term (Yeoh, 1993) to improve low strain accuracy.

In the applications to bridge/building bearings, solid rocket motor flexseals and off-shore structure flexjoints, rubber components are highly confined and the deformation is essentially bulk deformation. The work by Payne (1957), Gent and Lindley (1959), and Gent and Meinecke (1970) indicated that the mechanical behavior of highly confined rubber components is strongly affected by the magnitude of rubber bulk modulus, and therefore the "nearly incompressible" nature of rubber plays an important role in these applications. Finite element formulation that can accurately account for bulk deformation is critical to the analysis of this type of problems. Surely, pure incompressible finite element formulation is not applicable. Rubber under combined bending-shear deformation is also common in rubber mounting systems such as engine mounts and bushings. Varying the aspect ratio of rubber components changes the relative contributions of shear and bending to the overall deformation (Rivlin and Saunders, 1949) and thereby changes the structural stiffness. In this paper, the applicability of the present finite element method to these typical elastomeric problems is verified.

In the following, the numerical procedures of the pressure projection method are first presented in Section 2. The fundamental laboratory test problems, uniaxial tension-compression and simple shear, are analyzed in Section 3. These analyses also show how the Mooney-Rivlin model fails under large defamation. Two more incompressible finite elasticity problems, inflation and torsion problems, are analyzed in Section 4 to further illustrate the effectiveness of the proposed method. Some practical elastomeric applications such as bonded rubber units under tension and compression, and combined shear-bending example, together with an engine mount problem, are analyzed and compared to approximate solutions in Section 5.

2 Numerical Procedures

The pressure projection procedures and the corresponding nonlinear finite element formulation for nearly incompressible rubber-like materials were discussed in Part I (Chen et al., 1996). Recall the final incremental equilibrium equation

$$(\bar{\mathbf{K}} + \tilde{\mathbf{K}}^* + \tilde{\mathbf{K}}^{**})^{v+1}_{n+1}\Delta\mathbf{d} = \mathbf{f}^{\text{ext}}_{n+1} - (\bar{\mathbf{f}}^{\text{int}} + \tilde{\mathbf{f}}^{*\text{int}})^{v}_{n+1} \quad (2.1)$$

where n and v are load step and iteration counters, respectively.

Contributed by the Applied Mechanics Division of THE AMERICAN SOCIETY OF MECHANICAL ENGINEERS for publication in the ASME JOURNAL OF APPLIED MECHANICS.

Discussion on this paper should be addressed to the Technical Editor, Professor Lewis T. Wheeler, Department of Mechanical Engineering, University of Houston, Houston, TX 77204-4792, and will be accepted until four months after final publication of the paper itself in the ASME JOURNAL OF APPLIED MECHANICS.

Manuscript received by the ASME Applied Mechanics Division, May 8, 1995; final revision, Nov. 28, 1995. Associate Technical Editor: W. K. Liu.

The matrices $\bar{\mathbf{K}}$ and $\bar{\mathbf{f}}^{\text{int}}$ are associated with the distortional energy density $\bar{W}(\bar{I}_1, \bar{I}_2)$ and are independent of pressure projection. The matrices with superscript "*", $\tilde{\mathbf{K}}^*$ and $\tilde{\mathbf{f}}^{*\text{int}}$, are associated with the dilatational energy density $\tilde{W}(I_3)$ and therefore contain projected hydrostatic pressure quantity. The term $\tilde{\mathbf{K}}^{**}$ is resulting from the projection of hydrostatic pressure increment. The explicit expressions of the material response stiffness and geometric response stiffness in each of $\bar{\mathbf{K}}$ and $\tilde{\mathbf{K}}^*$ are given in Eqs. (3.40)–(3.43) in Part I.

Equation (2.1) is arranged for clarity and is computational inefficient if those matrices are formed separately. More efficient computational procedures are given below as follows:

1 Initialization.

2 Currently at the beginning of $(n+1)$th load step and $(v+1)$th iteration: d^v_{n+1} is known.

3 Compute kinematic variables: $(F_{ij})^v_{n+1}$, $(E_{ij})^v_{n+1}$, $(G^{-1}_{ij})^v_{n+1}$, $(\bar{I}_1)^v_{n+1}$, $(\bar{I}_2)^v_{n+1}$, $(I_3)^v_{n+1}$.

4 Compute the displacement calculated pressure $\partial\tilde{W}/\partial J$.

5 Form $(\mathbf{M}^e)^v_{n+1}$ and $(\mathbf{F}^e)^v_{n+1}$ (Eqs. (3.22) and (3.23) in Part I, respectively) and perform projection on hydrostatic pressure to obtain $(P^{e*})^v_{n+1}$ (Eq. (3.24) in Part I).

6 Compute $(\tilde{S}_{ij})^v_{n+1}$ (Eq. (3.4) in Part I) by replacing the displacement calculated hydrostatic pressure by $(P^{e*})^v_{n+1}$.

7 Compute $(\bar{S}_{ij})^v_{n+1}$ using Eq. (3.3) in Part I, and the total second Piola-Kirchhoff stress is

$$(S_{ij})^v_{n+1} = (\bar{S}_{ij})^v_{n+1} + (\tilde{S}_{ij})^v_{n+1}. \tag{2.2}$$

8 Form internal force vector $(\mathbf{f}^{\text{int}})^v_{n+1}$ by

$$(\mathbf{f}^{\text{int}})^v_{n+1} = \int_{\Omega^e_X} (\mathbf{B}^T_E \mathbf{Z})^v_{n+1} d\Omega \tag{2.3}$$

where $(\mathbf{Z})^v_{n+1}$ is the vector form of $(S_{ij})^v_{n+1}$.

9 Compute $(\tilde{T}_{ijkl})^v_{n+1}$ and $(\tilde{C}^1_{ijkl})^v_{n+1}$ (Eqs. (3.7) and (3.9) in Part I) using $(\tilde{S}_{ij})^v_{n+1}$ and the projected hydrostatic pressure $(P^{e*})^v_{n+1}$).

10 Calculate $(T_{ijkl})^v_{n+1}$ and $(C^1_{ijkl})^v_{n+1}$ by

$$(T_{ijkl})^v_{n+1} = (\bar{T}_{ijkl})^v_{n+1} + (\tilde{T}_{ijkl})^v_{n+1}, \tag{2.4}$$

$$(C^1_{ijkl})^v_{n+1} = (\bar{C}_{ijkl})^v_{n+1} + (\tilde{C}^1_{ijkl})^v_{n+1}. \tag{2.5}$$

where the explicit expressions of $(\bar{T}_{ijkl})^v_{n+1}$ and $(\bar{C}_{ijkl})^v_{n+1}$ are given in Eqs. (3.6) and (3.8) in Part I, respectively.

11 Form $(\tilde{\mathbf{R}}^e)^v_{n+1}$ and $(\tilde{\mathbf{M}}^e)^v_{n+1}$ (Eqs. (3.33) and (3.45) in Part I, respectively) and construct element stiffness matrix

$$(\mathbf{K}^e)^v_{n+1} = \int_{\Omega^e_X} (\mathbf{B}^T_F \mathbf{T} \mathbf{B}_F)^v_{n+1} d\Omega + \int_{\Omega^e_X} (\mathbf{B}^T_E \mathbf{C}^1 \mathbf{B}_E)^v_{n+1} d\Omega + k(\tilde{\mathbf{R}}^{eT})^v_{n+1} (\tilde{\mathbf{M}}^{e^{-1}})^v_{n+1} (\tilde{\mathbf{R}}^e)^v_{n+1}. \tag{2.6}$$

12 Solve global incremental equation:

$$(\mathbf{K})^v_{n+1} \Delta\mathbf{d} = (\mathbf{f}^{\text{ext}})_{n+1} - (\mathbf{f}^{\text{int}})^v_{n+1}. \tag{2.7}$$

13 Update displacement $\mathbf{d}^{v+1}_{n+1} = \mathbf{d}^v_{n+1} + \Delta\mathbf{d}$.

14 Convergence check.

In the present study, linear pressure fields, $\mathbf{Q} = \tilde{\mathbf{Q}} = [1, x, y]$ and $\mathbf{Q} = \tilde{\mathbf{Q}} = [1, x, y, z]$ are used in 9-node two-dimensional and 27-node three-dimensional Lagrangian elements, respectively.

3 Fundamental Test Problems

Three rubber models are used in this section: Mooney-Rivlin, Cubic, and Modified Cubic. The material constants fitted from uniaxial tensile data (Yeoh, 1990) are

(1) Mooney-Rivlin: $A_{10} = 0.2599$ Mpa, $A_{01} = 0.1608$ Mpa

(2) Cubic: $A_{10} = 0.373$ Mpa, $A_{20} = -0.031$ Mpa, $A_{30} = 0.005$ Mpa

(3) Modified Cubic: $A_{10} = 0.363$ Mpa, $A_{20} = -0.028$ Mpa, $A_{30} = 0.005$ Mpa, $\alpha = 0.123$ Mpa, $\beta = 10.1$.

For carbon black filled rubber, the bulk modulus to shear modulus ratio is around $10^4 \sim 10^5$ and therefore bulk modulus $k = 10^5$ Mpa is used in each material model. Nine-node and 27-node elements are used in two-dimensional and three-dimensional problems, respectively.

In this section, analyses and results are compared against analytical solutions and experimental data obtained from (Yeoh, 1990, 1993, 1994).

3.1 Uniaxial Tension-Compression. Since the stress-strain relation of uniaxial tension-compression is independent of cross-sectional geometry, a rubber block with dimension 1 cm × 1 cm × 4 cm is modeled by only one 27-node element in this analysis. The analytical solution can be found in Rivlin and Saunders (1951) as

$$\frac{t}{\lambda - \lambda^{-2}} = 2\left(\frac{\partial W}{\partial I_1} + \frac{1}{\lambda}\frac{\partial W}{\partial I_2}\right) \tag{3.1}$$

where t is the axial force divided by undeformed cross-sectional area, λ is the axial stretch ratio, and $t/(\lambda - \lambda^{-2})$ is called the reduced stress. In this problem, the rubber block is stretched up to 400 percent in axial tension and compressed down to 50 percent in axial compression. The finite element results calculated using different rubber models have excellent agreement with analytical solutions as shown in Fig. 1.

By the comparison with experimental data, one can observe that the Mooney-Rivlin model, which represents a linear relation between reduced stress and λ^{-1} in uniaxial deformation (as described in Eq. (3.1)), is not capable of capturing the upturn in the small strain region, and the nonlinearity beyond ~200 percent tension and ~20 percent compression. The finite element results obtained using the Cubic strain energy density function, on the other hand, agree quite well with experimental data in both large tension and compression but misses a certain amount of accuracy in the small strain region. The Modified Cubic function with an additional exponential term further improves small strain accuracy as shown in Fig. 1.

3.2 Shear of Rubber Component. A double-sandwich shear test problem is described in Fig. 2. When the width-to-thickness ratio (w/h) of the test specimen approaches infinity, rubber deforms in simple shear. The specimen used (Yeoh, 1990) has a width to thickness ratio of 4 and therefore only generates a "nearly" simple shear deformation. The analytical solution of simple shear can be found in Rivlin (1956) as

$$t = 2\left(\frac{\partial W}{\partial I_1} + \frac{\partial W}{\partial I_2}\right)\gamma \tag{3.2}$$

where t is shear stress and γ is shear strain. Note that Eq. (3.2) only provides an appropriate solution for this problem. Figure 2 indicates that the Mooney-Rivlin model, which contains only leading terms in I_1 and I_2, represents a linear shear stress-strain behavior as described in Eq. (3.2). The higher order models, such as the Cubic and Modified Cubic models, are more capable of characterizing the nonlinear shear stress-strain relation as shown in Fig. 2. Similar to the uniaxial deformation, the Modified Cubic strain energy density function further enhances the small strain accuracy when compared against experimental data.

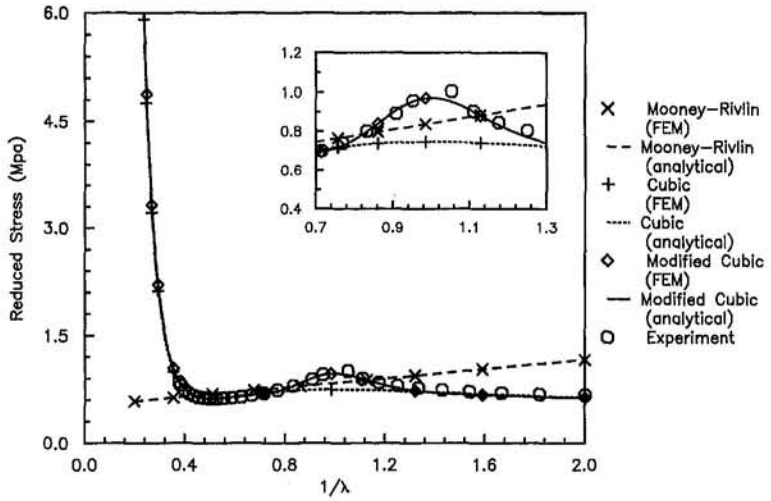

Fig. 1 Rubber block under uniaxial tension-compression: comparison of Mooney-Rivlin, Cubic, and modified Cubic strain energy density functions

The deformed shape at 200 percent shear strain is also plotted in Fig. 2. Due to the geometry of the test specimen, some small amount of bending deformation is observed near the edges.

4 Rubber Elasticity Problems

Since Modified Cubic strain energy density function differs from Cubic function simply at low strain as discussed in Section 3, only Mooney-Rivlin and Cubic strain energy density functions are used in this study.

4.1 Inflation of a Rubber Tube. Inflation is a good test problem for (nearly) incompressible finite element formulations because the pressure-displacement behavior is highly nonlinear and the hydrostatic pressure plays a significant role in this problem.

As described in Fig. 3, an infinitely long rubber cylinder, with inner radius of 6 cm and outer radius of 8 cm, is subjected to an internal pressure, p. The analytical solution of this problem can be derived from Rivlin (1949). For convenience, the analytical solution (considering only Mooney-Rivlin and Cubic strain energy density functions) is summarized as follows:

$$p(\rho) = (A_{10} + A_{01})[H_1(\rho, a_2) - H_1(\rho, a_1)] + A_{20}[H_2(\rho, a_2) - H_2(\rho, a_1)] + A_{30}[H_3(\rho, a_2) - H_3(\rho, a_1)] \quad (4.1)$$

where

$$H_1(\rho, a) = \ln\left(\frac{a^2}{a^2 + K(\rho)}\right) - \frac{K(\rho)}{a^2 + K(\rho)} \quad (4.2)$$

$$H_2(\rho, a) = -2\ln\left(\frac{a^2}{a^2 + K(\rho)}\right) + \left(\frac{K(\rho)}{a^2 + K(\rho)}\right)^2 - 2\frac{K(\rho)}{a^2} \quad (4.3)$$

$$H_3(\rho, a) = 6\ln\left(\frac{a^2}{a^2 + K(\rho)}\right) - \left(\frac{K(\rho)}{a^2 + K(\rho)}\right)^3 - \frac{3}{2}\left(\frac{K(\rho)}{a^2 + K(\rho)}\right)^2 - \frac{3}{2}\left(\frac{K(\rho)}{a^2}\right)^2 + 6\frac{K(\rho)}{a^2} \quad (4.4)$$

$$K(\rho) = \rho^2 - a_2^2 \quad (4.5)$$

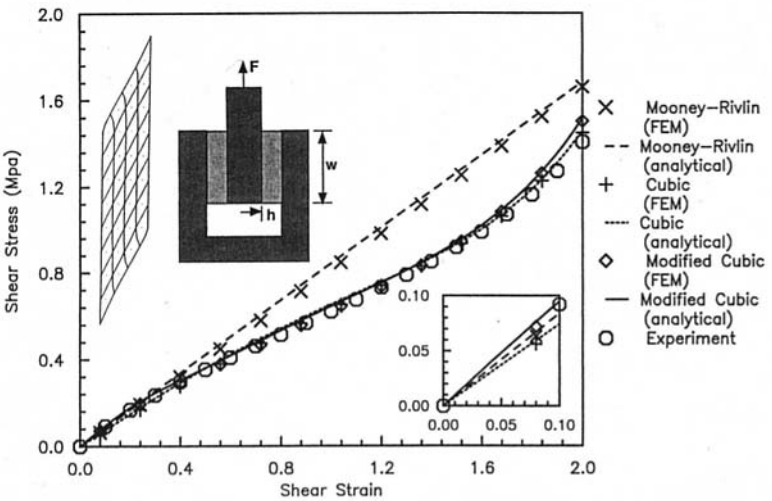

Fig. 2 Rubber block under simple shear deformation: comparison of Mooney-Rivlin, Cubic, and modified Cubic strain energy density functions

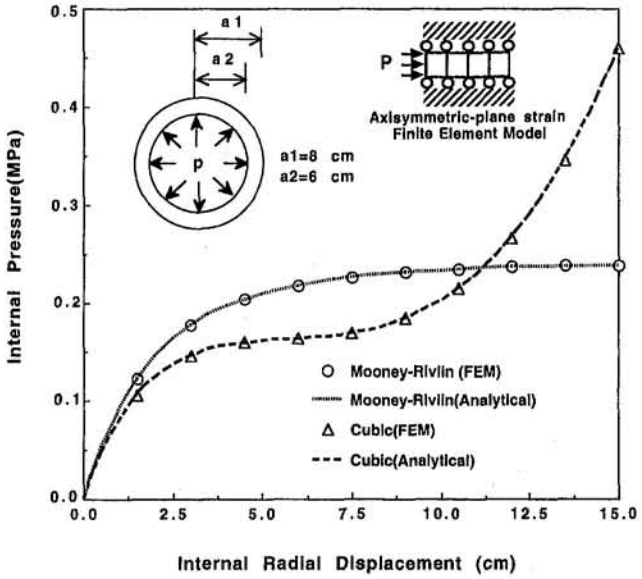

Fig. 3 Rubber cylinder subjected to internal pressure: comparison of load-displacement response using Mooney-Rivlin and Cubic models

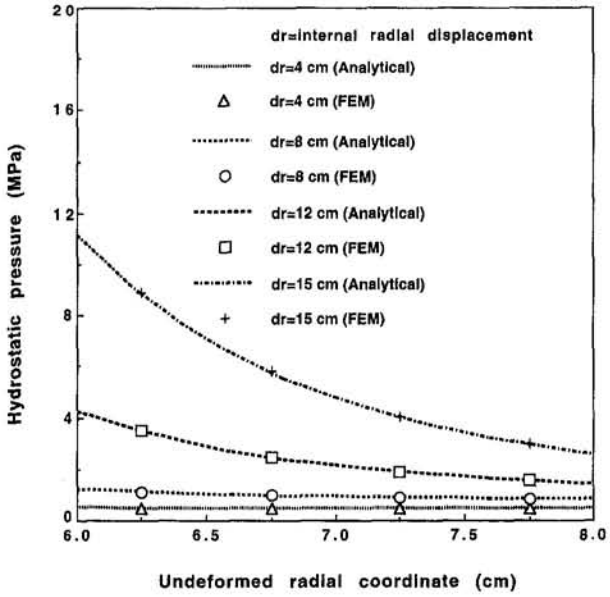

Fig. 4 Rubber cylinder subjected to internal pressure: comparison of hydrostatic pressure calculated from finite element and analytical solution using Cubic rubber model

and a_1 and a_2 are the outer and inner radius of the undeformed cylinder, respectively, ρ is the inner radius of the deformed cylinder, and p is the internal pressure.

This problem is modeled by four axisymmetric 9-node elements with restraints in the axial direction to reflect the plane-strain condition in the axial direction, as shown in Fig. 3. As described in Eqs. (4.1)–(4.5), a limit pressure exists if the Mooney-Rivlin model is used, i.e.,

$$P(\rho)|_{\rho\to\infty} = 2(A_{10} + A_{01}) \ln \frac{a_2}{a_1} = 0.2405 \text{ Mpa}. \quad (4.6)$$

Displacement control is used in this analysis and a total of ten steps are used to inflate the inner radius of the tube from 6 cm to 21 cm. The finite element and analytical pressure-displacement curves obtained using a Mooney-Rivlin material are compared in Fig. 3. The corresponding internal pressure at the final deformed stage is 0.23919 Mpa which is equivalent to 99.5 percent of the limit pressure. The error of finite element solution is 0.014 percent at the final deformed stage. The Cubic material model, compared to Mooney-Rivlin, demonstrates a different load-deflection characteristic, as shown in Fig. 3, due to the contribution of the higher order terms in the strain energy density function. In this analysis, 0.3 percent error is generated by the present finite element solution at the final deformed stage. The hydrostatic pressure distributions at various deformation states are plotted in Fig. 4 and results are satisfactory.

4.2 Simple Torsion of a Solid Rubber Cylinder. A simple torsion is generated by rotating the two end surfaces of a solid cylinder in their own planes about the axis of the cylinder without axial motion. This problem discusses the amount of axial force needed to be applied to the twisted rubber cylinder in order to maintain it in simple torsion. The solution of this problem has been discussed by Rivlin (1949) where the resulting force N acting along the axis of the cylinder is given by

$$N = \pi\phi^2 \int_0^a 2r^3 \left(\frac{\partial W}{\partial I_1} + 2\frac{\partial W}{\partial I_2} \right) dr \quad (4.7)$$

where ϕ is the amount of torsional angle per unit length and a is the radius of the cylinder. The dimension of this problem is described in Fig. 5. Since the twisted angle per unit axial length in simple torsion is constant, only one layer of elements is used in the axial direction. A total of 48 27-node elements, as shown in Fig. 5, are used in this problem.

The axial forces calculated by finite element using Mooney-Rivlin and Cubic strain energy density functions are compared against analytical solutions in Fig. 5. The agreement between finite element and analytical solutions is good. The axial stress distributions at various deformed states calculated using the Cubic model are plotted in Fig. 6 and the results are satisfactory. In this problem, as can be understood from Eq. (4.7), that the initial slope of the $N - \theta$ curve is proportional to $C_{10} + 2C_{01}$. Hence, the Mooney-Rivlin model demonstrates a stiffer response compared to that of the Cubic model, as shown in Fig. 5.

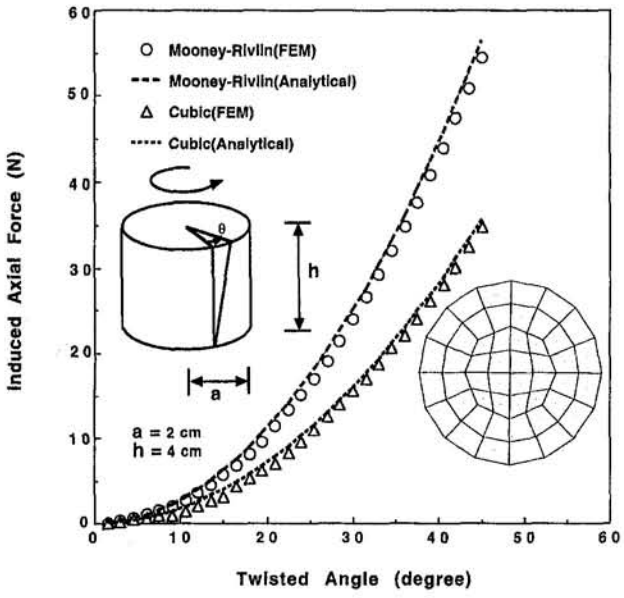

Fig. 5 Rubber solid cylinder subjected to simple torsion: comparison of induced axial force versus twisted angle using Mooney-Rivlin and Cubic models

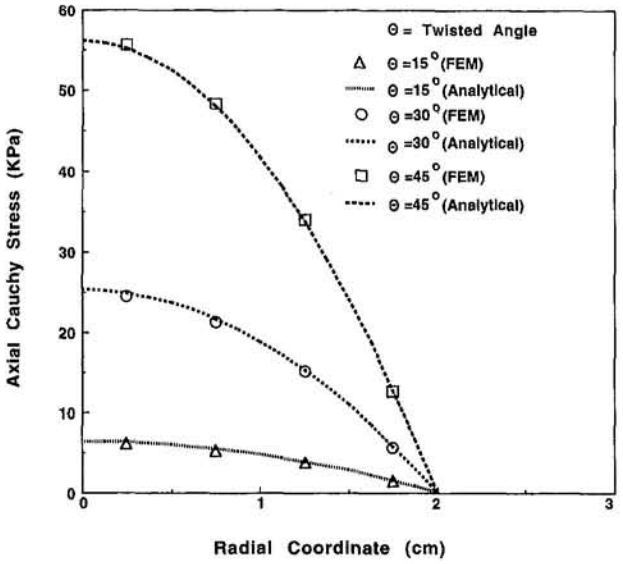

Fig. 6 Rubber solid cylinder subjected to simple torsion: comparison of axial stress distribution calculated from finite element and analytical solution using Cubic model

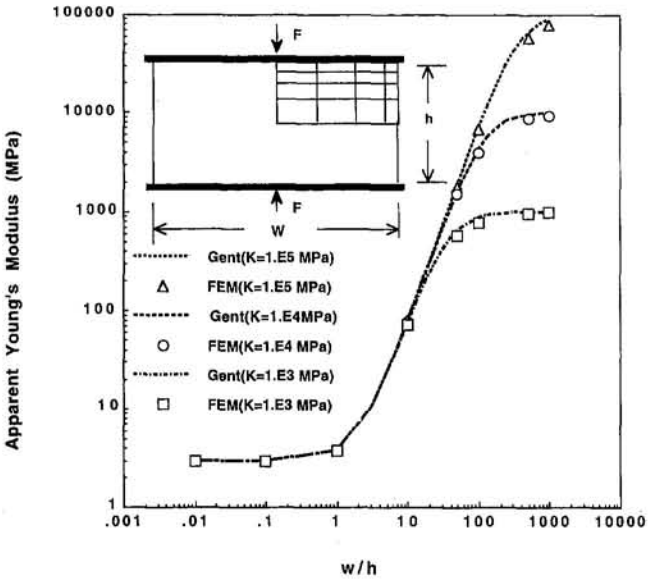

Fig. 8 Plane-strain bonded rubber unit under compression: effect of width/height ratio on the apparent Young's modulus

5 Application to Engineering Elastomers

The study in Section 3 indicates that the Cubic strain energy density is more appropriate for large and complex deformation problems. Only Cubic strain energy density function is considered in problems 5.1 and 5.2. The problem definition of example 5.3 is taken from Tseng et al. (1987) where material constants were characterized using the Mooney-Rivlin model.

5.1 Bulk Deformation of Bonded Rubber. The mechanical behavior of bonded rubber under compression has been studied since the 1950s by Payne (1957), Gent and Lindley (1959), Gent and Meinecke (1970), and others by using the concept of "apparent Young's modulus." In their work, the apparent Young's modulus for a bonded rubber unit was estimated from the Young's modulus of an unbonded rubber unit in conjunction with the shape effect. Based on small deformation assumption, the force-displacement relation of a bonded rubber unit can be described by

$$F = E_a A_0 e \tag{5.1}$$

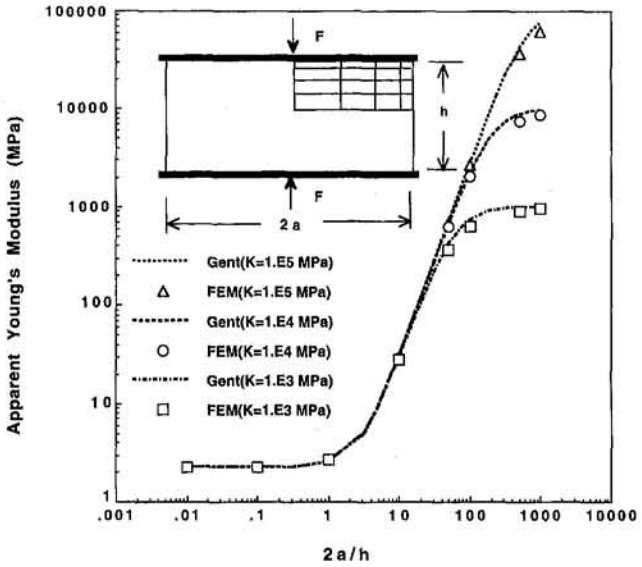

Fig. 7 Axisymmetric bonded rubber unit under compression: effect of width/height ratio on the apparent Young's modulus

and

$$E_a = E_u(1 + \beta S^2) \tag{5.2}$$

where A_0 is the undeformed cross sectional area, e is the compressive (tensile) axial strain, $\beta = 2$ for axisymmetric case and $\beta = 1$ for plane-strain case, S is the shape factor defined by the ratio of loaded area to unloaded area, E_a is called the apparent Young's modulus and E_u is the Young's modulus of unbonded rubber components:

$$E_u = \alpha\left(\frac{\partial W}{\partial I_1} + \frac{\partial W}{\partial I_2}\lambda^{-1}\right)\Big|_{I_1=I_2=3}, \tag{5.3}$$

where $\alpha = 6$ for axisymmetric case and $\alpha = 8$ for plane-strain case with λ^{-1} dropped. Gent also mentioned that rubber is not fully incompressible and the bulk modulus, k, should be considered in the deformation of rubber, especially when the rubber unit is very thin and bonded. The apparent Young's modulus E_a in Eq. (5.1) should be replaced by $E_{a'}$ in the following form:

$$\frac{1}{E_{a'}} = \frac{1}{E_a} + \frac{1}{k}. \tag{5.4}$$

The finite element method is used to study this problem. For

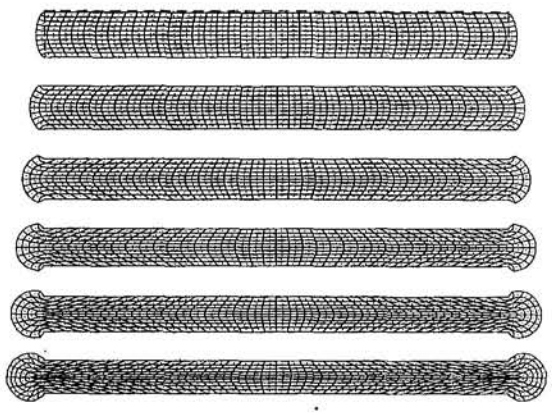

Fig. 9 Deformed geometries of axisymmetric bonded rubber unit under compression

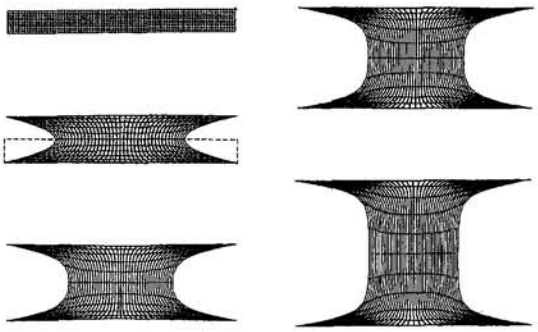

Fig. 10 Deformed geometries of axisymmetric bonded rubber unit under tension

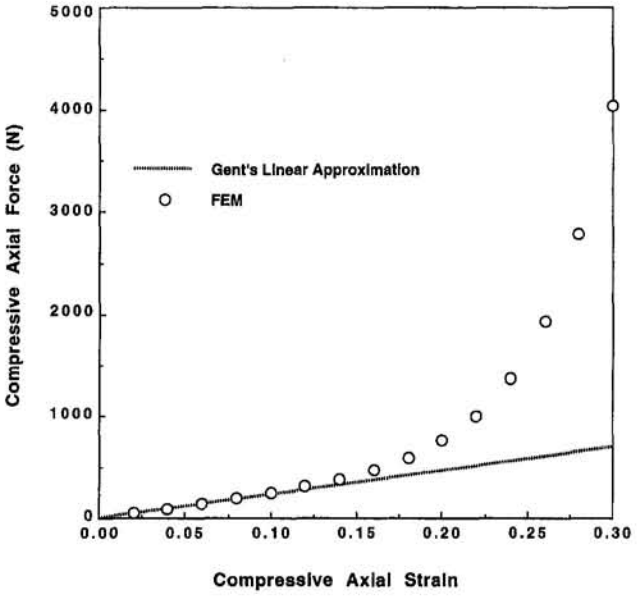

Fig. 11(*a*) Load-deflection curve of axisymmetric rubber unit under compression: comparison of finite element solution and Gent's linear approximation

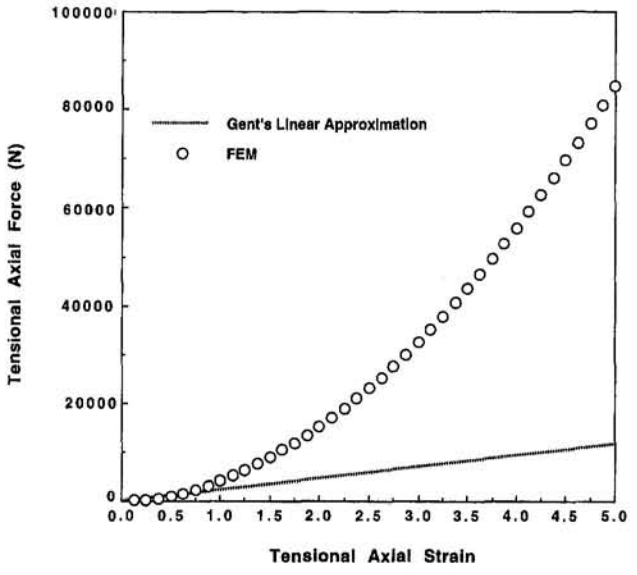

Fig. 11(*b*) Load-deflection curve of axisymmetric rubber unit under tension: comparison of finite element solution and Gent's linear approximation

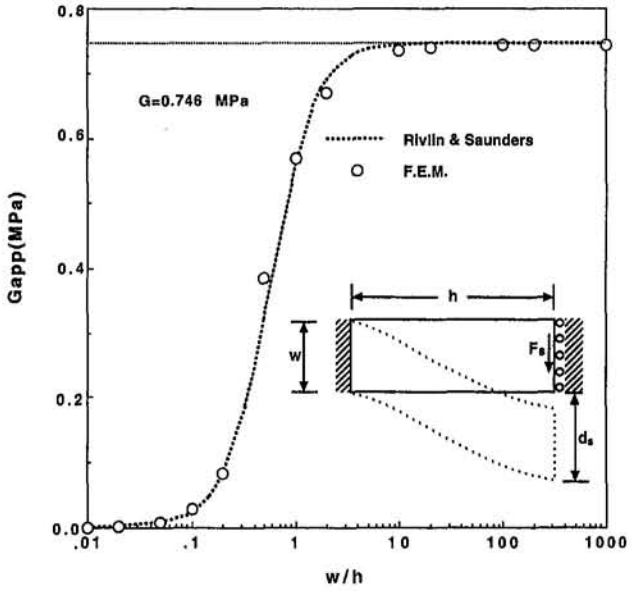

Fig. 12 Plane-strain rubber component under shear and bending deformation: effect of structural geometry on the apparent shear modulus

the comparison with Gent's approximation, linear analysis is first performed. In this problem, rubber behavior is described by the Cubic strain energy density function and a mesh of 4 × 4 nine-node elements, as shown in Fig. 7, are used in the finite element analysis. Three arbitrarily selected bulk moduli, 1×10^3, 1×10^4, 1×10^5 Mpa (representing bulk modulus to shear modulus ratios of 1.34×10^3, 1.34×10^4, 1.34×10^5, respectively) are used to study the effect of bulk modulus on the structural stiffness. In this study, the width/height ratio of the rubber units varies from 0.01 to 1000. The finite element results are compared against Gent's approximation in Figs. 7–8 for axisymmetric and plane-strain cases, respectively, and very good agreement is observed. In the small width/height range, the apparent Young's modulus approaches that of the unbonded case. As the width/height ratio becomes very large, the apparent Young's modulus approaches to bulk modulus and this deformation is called bulk compression (tension).

Large deformation analysis of bonded rubber with $k = 10^4$ Mpa under tension and compression are also performed. An axisymmetric rubber unit with diameter to height ratio of 10 is used in the analysis. Five and 20 elements in the axial and radial directions, respectively, are used to model one quarter of the structure. In the compression analysis, rubber squeezes out at the edges as shown in Fig. 9 and the analysis terminated when the rubber is compressed more than 30 percent of the original thickness, due to excessive mesh entanglement. In the tension analysis, rubber is stretched up to five times the original thickness and the deformed geometries are plotted in Fig. 10. The nonlinear finite element load-displacement curves are also compared against Gent's linear approximate solution in Figs. 11(*a*) and 11(*b*) for compression and tension, respectively. The highly nonlinearities predicted by finite element suggested that Gent's solution is applicable only at around 50 percent strain in tension and around 15 percent strain in compression in this problem.

This problem also demonstrates the need of using a nearly incompressible formulation for rubber that is not purely incompressible. As indicated in Figs. 7–8, the magnitude of bulk modulus determines the structural stiffness in bonded thin rubber components. The finite element formulation that can accurately captures bulk deformation is essential to the success in the analysis of highly confined engineering elastomers. The present formulation decouples the distortional and dilatational

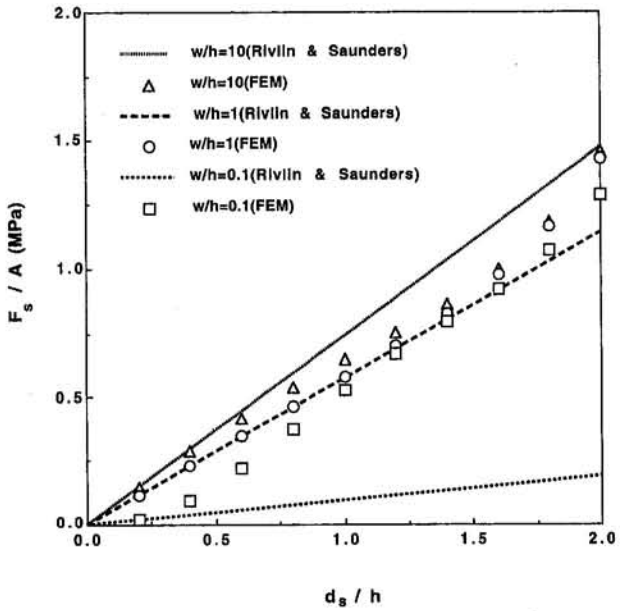

Fig. 13 Load-deflection curves of plane strain rubber component under shear and bending deformation: comparison of finite element solution and linear approximation by Rivlin and Saunders

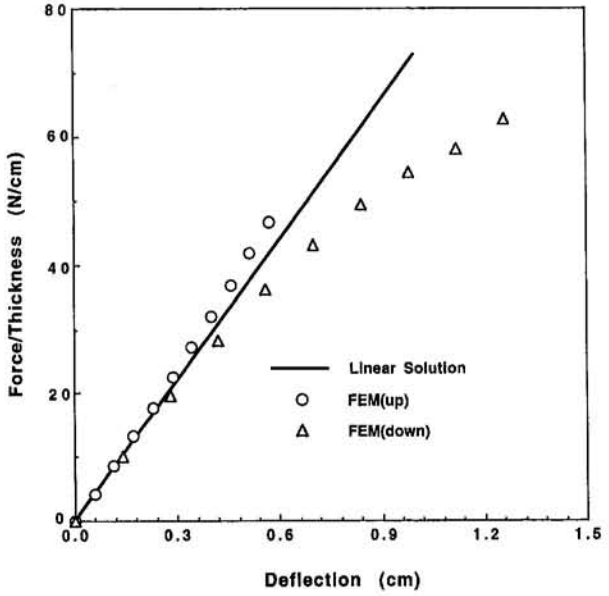

Fig. 15 Load-deflection characteristics of engine mount under vertical load: comparison of finite element results and linear approximation

strain energy and therefore performs quite well in this analysis as shown in Figs. 7–8.

5.2 Combined Shear and Bending of Rubber Components. Rivlin and Saunders (1951) considered the deformation to result from the sum of a simple shear deformation and a bending deformation based on small deformation theory, and proposed an apparent shear modulus given by

$$G_{\text{app}} = G/\left(1 + \frac{h^2}{36K^2}\right) \tag{5.5}$$

$$G = 2\left(\frac{\partial W}{\partial I_1} + \frac{\partial W}{\partial I_2}\right)\Big|_{I_1=I_2=3} \tag{5.6}$$

where K is the radius of gyration, G is the shear modulus, and h is defined in Fig. 12 where the problem definition is given. The finite element nodes on the left end are totally fixed and those on the right end are restrained in the horizontal direction and are forced to move with the same amount of vertical displacement. Plane-strain rubber components with w/h ranging from 0.01 to 1000 (w is fixed as 1 cm) are included in the analysis. Total of 20 × 6 9-node elements are used in the analysis. The finite element apparent shear modulus is calculated by

$$G_{\text{app}} = \frac{F_s h}{A d_s} = (F_s/A)/(d_s/h) \tag{5.7}$$

where F_s and d_s are defined in Fig. 12 and A is the rubber cross-sectional area. The finite element results agree well with

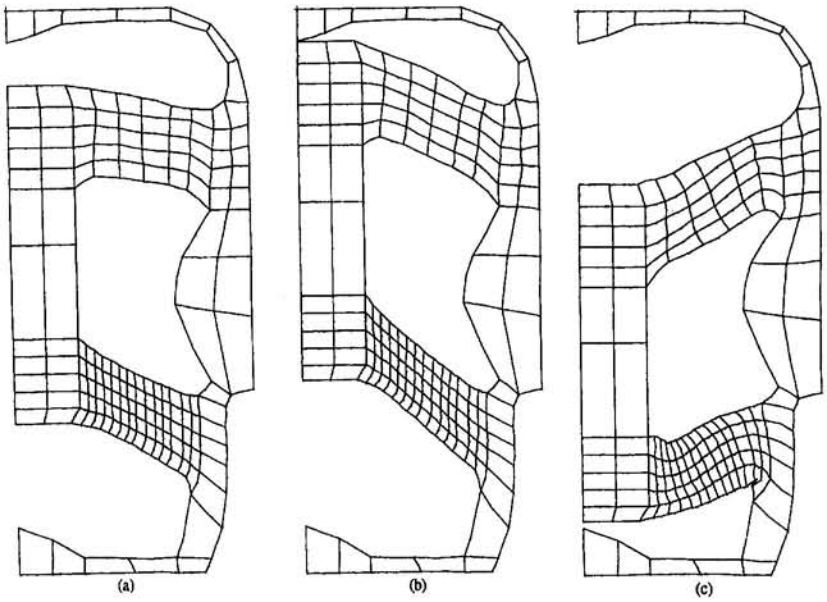

Fig. 14 Undeformed and deformed geometries of engine mount under vertical upward and downward loading

solutions provided by Rivlin and Saunders shown in Fig. 12. When w/h is small, the deformation is primarily in bending and therefore the apparent shear modulus is low. On the other hand, a thin rubber unit with very high w/h value deforms essentially in shear and hence the apparent shear modulus approaches to the shear modulus of rubber.

The nonlinear shear-bending behavior of the rubber unit with $w = 1$ cm and w/h equal to 0.1, 1, 10 is also studied. The nonlinear load-deflection curves predicted by finite element are compared against the linear approximation obtained from Eq. (5.5) in Fig. 13. As indicated in Fig. 13, when deflection is small, rubber unit with $w/h = 0.1$ deforms primarily in bending and the corresponding apparent shear modulus is much lower than that of the other two units. While at large deflection, due to the boundary conditions imposed on the right end of the structure, all three rubber units deform primarily in shear and therefore exhibit similar apparent shear moduli at large strain.

5.3 Analysis of Engine Mount. This engine mount problem is taken from Tseng et al. (1987) (shown in Fig. 14(a)) where rubber was characterized using the Mooney-Rivlin model with $A_{10} = 0.145$ Mpa and $A_{01} = 0.062$ Mpa. Since only limited raw stress-strain data were provided, we did not to recharacterize rubber properties using the Cubic model.

The outer metal box of the engine mount is connected to the car body, therefore the outer metal/rubber interface is totally fixed in the finite element model. The inner metal piece is attached to the engine and, hence, the external load is applied to the inner metal. In this example, the vertical load-deflection characteristic of the engine mount is analyzed.

When vertical load is applied to the inner metal, only half of the structure is modeled, due to symmetry. With a longer travel distance in the downward motion than in the upward motion, the lower rubber leg is expected to undergo large and complicated deformation; and, therefore, a finer mesh is used to model the lower rubber leg. Figure 14 shows that the rubber legs are under a combination of compression (tension), shear and bending deformation. Some localized buckling occurs near the lower right corner of the lower rubber leg. The finite element load-deflection curves are compared against the linear solution obtained from Eqs. (5.1)–(5.7) in Fig. 15. The finite element solution correlates well with the linear approximation at small deformations. The nonlinear load-deflection behavior is due to the severe bending and shear in the rubber components as have discussed in the previous examples.

6 Conclusions

The purpose of this paper is to demonstrate the performance of the present method and to study some of the typical structural characteristics of engineering elastomers using the present method in conjunction with several strain energy density functions. Numerical procedures of the projection method that can be implemented into displacement based finite element programs is presented. A series of numerical examples demonstrate the performance of the present method.

The comparison of finite element analysis results with experimental data in tension-compression and shear suggests that the higher order strain energy density functions are required to capture stress-strain nonlinearities. In the problems with strong boundary constraints, the structural stiffness is largely depending on the magnitude of rubber bulk modulus. This type of analysis requires a finite element formulation that is capable of capturing the bulk deformation of rubber. With the decomposition of the strain energy density function and the use of pressure projection method, the present formulation performs effectively in these classical finite elasticity problems as well as bulk deformation problems.

References

Chang, T. Y. P., Saleeb, A. F., and Li, G., 1991, "Large Strain Analysis of Rubber-like Materials Based on a Perturbed Lagrangian Variational Principle," *Computational Mechanics,* Vol. 8, pp. 221–233.

Chen, J. S., and Pan, C., 1996, "A Pressure Projection Method for Nearly Incompressible Rubber Hyperelasticity, Part I: Theory," ASME JOURNAL OF APPLIED MECHANICS, Vol. 63, pp. 862–868.

Gent, A. N., and Lindley, P. B., 1959, "The Compression of Bonded Rubber Blocks," *Proceedings of the Institution of Mechanical Engineers,* Vol. 173, pp. 111–122.

Gent, A. N., and Meinecke, E. A., 1970, "Compression, Bending and Shear of Bonded Rubber Blocks," *Polymer Engineering and Science,* Vol. 10, pp. 48–53.

James, A. G., Green, A., and Simpson, G. M., 1975a, "Strain Energy Functions of Rubber. I. Characterization of Gum Rubber," *Journal of Applied Polymer Science,* Vol. 19, pp. 2033–2058.

James, A. G., and Green, A., 1975b, "Strain Energy Functions of Rubber. II. The Characterization of Filled Vulcanizates," *Journal of Applied Ploymer Science,* Vol. 19, pp. 2319–2330.

Liu, W. K., Belytschko, T., and Chen, J. S., 1988, "Nonlinear Versions of Flexurally Superconvergent Elements," *Computer Methods in Applied Mechanics and Engineering,* Vol. 71, pp. 241–256.

Payne, A. R., 1957, "Dynamic Properties of Vulcanized Rubber: 5. Shape Factors and Functions in Rubber Engineering," *Research Association of British Rubber Manufactures,* Research Report No. 84, Shawbury.

Rivlin, R. S., 1949, "Large Elastic Deformation of Isotropic Materials, Part VI, Further Results in the Theory of Torsion, Shear and Flexure," *Philosophical Transactions of the Royal Society of London,* Vol. A242, pp. 173–195.

Rivlin, R. S., 1956, "Rheology Theory and Applications," F. R. Eirich, ed., Academic Press, New York, Vol. 1, Chapter 10, pp. 351–385.

Rivlin, R. S., and Saunders, D. W., 1951, "Large Elastic Deformation of Isotropic Materials. Part 7, Experiments on the Deformation of Rubber," *Philosophical Transactions of the Royal Society of London,* Vol. A243, pp. 251–288.

Rivlin, R. S., and Saunders, D. W., 1949, "Cylindrical Shear Mountings," *Transactions, I.R.I.,* Vol. 24, p. 296.

Scharnhorst, T., and Pian, T. H. H., 1978, "Finite Element Analysis of Rubber-like Materials by a Mixed Model," *International Journal for Numerical Methods in Engineering,* Vol. 12, pp. 665–676.

Tschoegl, N. W., 1971, "Constitutive Equations for Elastomers," *Journal of Applied Ploymer Science,* Vol. A1, pp. 1959–1970.

Tseng, N. T., Satyamurthy, K., and Chang, J. P., 1987, "Nonlinear Finite Element Analysis of Rubber Based Products," The 131st Meeting of the Rubber Division, American Chemical Society, Montreal, Quebec, Canada, May 26–29.

Yeoh, O. H., 1990, "Characterization of Elastic Properties of Carbon Black Filled Rubber Vulcanizates," *Rubber Chemistry and Technology,* Vol. 63, pp. 792–805.

Yeoh, O. H., 1993, "Some Forms of the Strain Energy Function for Rubber," *Rubber Chemistry and Technology,* Vol. 66, pp. 754–771.

Yeoh, O. H., 1994, personal communication.